Research Article

For reprint orders, please contact: reprints@futuremedicine.com

Nanomedicine

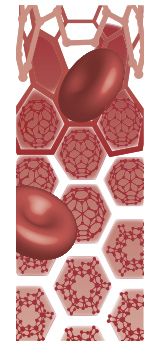

Sulfobetaine methacrylate-albumin-coated graphene oxide incorporating IR780 for enhanced breast cancer phototherapy

Bruna L Melo[1], Rita Lima-Sousa[1], Cátia G Alves[1], Paula Ferreira[2], André F Moreira[1], Ilídio J Correia**[,1,2] & Duarte de Melo-Diogo*[,1]

[1]CICS-UBI – Centro de Investigação em Ciências da Saúde, Universidade da Beira Interior, Avenida Infante D. Henrique, Covilhã 6200–506, Portugal

[2]CIEPQPF – Departamento de Engenharia Química, Universidade de Coimbra, Rua Silvio Lima, Coimbra 3030–790, Portugal

*Author for correspondence: demelodiogo@fcsaude.ubi.pt

**Author for correspondence: Tel.: +351 275 329 055; icorreia@ubi.pt

Aim: Enhance the colloidal stability and photothermal capacity of graphene oxide (GO) by functionalizing it with sulfobetaine methacrylate (SBMA)-grafted bovine serum albumin (BSA; i.e., SBMA-*g*-BSA) and by loading IR780, respectively. **Materials & methods:** SBMA-*g*-BSA coating and IR780 loading into GO was achieved through a simple sonication process. **Results:** SBMA-*g*-BSA-functionalized GO (SBMA-BSA/GO) presented an adequate size distribution and cytocompatibility. When in contact with biologically relevant media, the size of the SBMA-BSA/GO only increased by 8%. By loading IR780 into SBMA-BSA/GO, its photothermal capacity increased by twofold. The combination of near infrared light with SBMA-BSA/GO did not induce photocytotoxicity on breast cancer cells. In contrast, the interaction of IR780-loaded SBMA-BSA/GO with near infrared light caused the ablation of cancer cells. **Conclusion:** IR780-loaded SBMA-BSA/GO displayed an improved colloidal stability and phototherapeutic capacity.

First draft submitted: TBC; Accepted for publication: TBC; Published online: 4 March 2021

Keywords: 2D materials • cancer therapy • graphene nanomaterials • photothermal therapy • protein-based coatings • zwitterionic coatings

Nanomaterials have been extensively investigated for cancer-related applications due to their ability to passively accumulate at the tumor site [1,2]. Owing to this feature and depending on the nanomaterials' intrinsic properties, they can be used for a myriad of therapeutic or imaging modalities [1,3–5]. For therapeutic applications, nanostructures with near infrared (NIR; 750–1000 nm) light absorption (e.g., gold nanorods [6], CuS nanoparticles [7] and polydopamine nanostructures [8]) have been capturing the attention of researchers. In this regard, graphene oxide (GO) nanomaterials are promising candidates due to their NIR absorption and loading capacity [9–11]. Upon interaction with NIR light, GO can produce a temperature increase (ΔT) that causes damage to cancer cells (photothermal therapy [PTT]) [12–15]. In cancer PTT, the use of NIR light is fundamental due to its minimal/insignificant interaction with biological components (e.g., hemoglobin, melanin and water), ensuring a high tissue penetration depth and minimal off-target heating [1,16]. Additionally, GO presents an aromatic lattice that can encapsulate hydrophobic molecules through noncovalent interactions, endowing it with drug delivery capabilities [13,17,18]. The nanomaterials' photothermal heating can also trigger other events (e.g., drug release [18–20]), paving the way for the development of multifunctional nanoagents. Moreover, it has been recently suggested the use of nanomaterials' photothermal effect for the elimination of pathogens from respiratory protective equipment [21].

Despite its NIR responsiveness, the poor colloidal stability of GO limits its direct application for cancer PTT [9,22,23]. Upon contact with biological fluids, as-synthesized GO precipitates, undermining its capacity to reach the tumor site [9,10,23]. To address this limitation, GO derivatives have been functionalized with PEG-based coatings [10,23,24]. However, a recent study has unveiled that systemically administered PEGylated GO derivatives suffer from the so-called accelerated blood clearance (ABC) phenomenon [25]. In brief, anti-PEG antibodies are generated at the time of the first intravenous injection of the PEGylated nanomaterials, which in turn mediate the rapid clearance of these nanostructures in subsequent injections [25]. This phenomenon has also been reported for

Future Medicine

other types of PEGylated nanomaterials, including for US FDA/EMA approved nanomedicines (e.g., Caelyx) [26–29]. Therefore, it is of utmost importance to develop new coatings that can improve the colloidal stability of GO.

On the other hand, PTT based on GO nanomaterials requires the administration of high doses or the use of intense radiation in order to attain a suitable therapeutic effect [30–33]. Therefore, the subpar photothermal capacity of GO is also an impediment for its broader use in cancer PTT. To overcome this bottleneck, GO can be reduced with hydrazine hydrate, a process that restores its graphitic lattice, improving its NIR absorption and hence its photothermal capacity [34,35]. For example, Robinson *et al.* prepared hydrazine hydrate-reduced GO that displayed a 6.8-times higher NIR absorption and a 2.2-times greater photothermal capacity than GO [35]. However, hydrazine hydrate-reduced GO presents a poor cytocompatibility due to the toxicity of this reducing agent [36]. Reduced GO nanoribbons [37] and reduced GO nanomeshes [38] can display an even greater NIR absorption. Nevertheless, the production of these derivatives also relies on the use of hydrazine. Alternatively, environment friendly methods have also been proposed to reduce GO (e.g., using bacteriorhodopsin [39], green tea [40], glucose [41] and curcumin [42]). However, these methods are not yet widely applied since the environment friendly reduced GO still requires further biological characterization. In turn, other NIR-responsive nanomaterials (e.g., gold nanorods [43], iron oxides [11], zinc ferrite spinels [44] and copper sulfides [20]) can be grown directly on the aromatic lattice of GO, improving its photothermal capacity. Nevertheless, the formulation of these nanohybrids is a complex process, limiting their large-scale assembly and future translation [45–47].

In this work, and for the first time, GO was functionalized with a protein based amphiphilic coating containing sulfobetaine methacrylate (SBMA) brushes, and was loaded with IR780, with the intent to improve its colloidal stability and photothermal capacity, respectively. In a previous report, it was demonstrated that polymeric nanoparticles formulated using SBMA-grafted bovine serum albumin (BSA) (i.e., SBMA-*g*-BSA) display an improved colloidal stability and enhanced cellular uptake [48]. Furthermore, SBMA-functionalized nanomaterials have also a long blood circulation time, thereby achieving a high tumor uptake [49]. As importantly, SBMA-coated nanoparticles are not reported to suffer from the ABC phenomenon [50]. On the other hand, IR780 (a hydrophobic small molecule) was selected to be loaded on the graphitic lattice of GO due to its high NIR absorption [48,51]. Furthermore, the optical properties of IR780 are superior or equivalent to those displayed by other NIR responsive dyes such as indocyanine green and other prototypic heptamethine cyanines (e.g., IR775, IR783, IR797 and IR806) [52].

SBMA-*g*-BSA-functionalized GO (SBMA-BSA/GO) was obtained through a simple sonication process, and it displayed an adequate size distribution and cytocompatibility for cancer-related applications. When in contact with biologically relevant media, the size of the SBMA-functionalized GO derivatives only increased by 8% after 48 h, revealing an excellent colloidal stability. In the same conditions, GO (without any functionalization) and non-SBMA-functionalized GO (BSA-coated GO) suffered a 63 and 31% increase in their size, respectively. By loading IR780 into SBMA-BSA/GO (IR/SBMA-BSA/GO), the nanomaterials' NIR absorption increased by 5.6-fold. In this way, the IR/SBMA-BSA/GO could produce an up to two-times higher photoinduced heat than SBMA-BSA/GO. In the *in vitro* studies, the combination of NIR light with SBMA-BSA/GO did not induce photocytotoxicity on breast cancer cells. In stark contrast, the interaction of IR/SBMA-BSA/GO with NIR light caused the ablation of cancer cells (cell viability <2%). Overall, IR/SBMA-BSA/GO displays a greatly improved colloidal stability and phototherapeutic capacity, being a promising nanohybrid for application in the PTT of breast cancer cells.

Materials & methods

Materials

DMEM-F12, IR780, DL-Dithiothreitol (DTT) and SBMA were purchased from Sigma–Aldrich (Sintra, Portugal). Methanol was obtained from Honeywell (Oeiras, Portugal). BSA was obtained from Amresco (PA, USA). 3-(4,5-dimethylthiazol-2-yl)-5-(3-carboxymethoxyphenyl)-2-(4-sulfophenyl)-2H-tetrazolium (MTS) was bought from Promega (WI, USA). Michigan Cancer Foundation-7 (MCF-7) cell line was acquired from ATCC (Middlesex, UK). Normal human dermal fibroblasts (NHDF) were obtained from PromoCell (Heidelberg, Germany). Fetal bovine serum (FBS) was bought from Biochrom AG (Berlin, Germany). Calcein-AM, cell culture plates, T-flasks and propidium iodide (PI) were purchased from Thermo Fisher Scientific (Porto, Portugal). Cell imaging plates were obtained from Ibidi GmbH (Munich, Germany). GO was acquired from NanoPoz (Umultowska Poznan, Wielkopolska). SBMA-*g*-BSA was synthesized as previously described [48]. Water used in all assays was double deionized (0.22 μm filtered; 18.2 MΩ cm).

Methods

Production of SBMA-BSA/GO & IR/SBMA-BSA/GO

IR/SBMA-BSA/GO was produced by adapting protocols previously described [13,48]. Initially, SBMA-*g*-BSA (0.09 mg/ml; 1 ml) and DTT (0.005 mg/ml, 1 ml) were allowed to react for 20 min under constant stirring [48]. Then, GO (200 µg/ml; 0.5 ml) was mixed with the polymer-DTT solution (0.5 ml) and sonicated for 60 min (Branson 5800; Branson Ultrasonics, CT, USA). Subsequently, IR780 (20 µg in methanol) was added to the previous solution, followed by another 30 min of sonication. This solution was then dialyzed against water (500–1000 Da molecular weight cut-off membrane) for 90 min to remove DTT, methanol and nonloaded IR780. Finally, the recovered solution was centrifuged to remove any aggregates, yielding IR/SBMA-BSA/GO. To produce SBMA-BSA/GO, the process was the same but without the IR780 addition step. As control, BSA-functionalized GO (BSA/GO) was also produced as described above using BSA instead of SBMA-*g*-BSA.

Characterization of SBMA-g-BSA, GO, SBMA-BSA/GO & IR/SBMA-BSA/GO

The successful synthesis of SBMA-*g*-BSA was confirmed by Fourier transform infrared spectroscopy (FTIR) using a Nicolet iS10 spectrometer (Thermo Scientific, Inc., MA, USA). The physicochemical properties of GO were confirmed by FTIR, UV-visible absorption spectroscopy (Evolution 201 spectrophotometer; Thermo Scientific, Inc.) and energy-dispersive x-ray spectroscopy (XFlash Detector 5010; Bruker, Karlsruhe, Germany). SBMA-BSA/GO and IR/SBMA-BSA/GO size distribution and zeta potential were evaluated in a Zetasizer Nano ZS (Malvern Instruments Ltd., Worcestershire, UK). The variation of IR/SBMA-BSA/GO, SBMA-BSA/GO, BSA/GO and GO size over time when dispersed in cell culture medium (DMEM-F12 with 10% [v/v] of FBS) was also investigated [48]. The dimensions of GO, SBMA-BSA/GO and IR/SBMA-BSA/GO were confirmed by transmission electron microscopy (TECNAI G2 20 S-TWIN [FEI Company, The Netherlands]; operated at an accelerating voltage of 200 kV). Prior to this analysis, the samples were stained with phosphotungstic acid (2% [w/v]). Visible-NIR absorption spectroscopy was employed to confirm the NIR absorption of SBMA-BSA/GO and IR/SBMA-BSA/GO and the IR780 encapsulation efficiency. Initially, the absorption of IR/SBMA-BSA/GO at 890 nm, when dispersed in water, was analyzed. Then, a standard curve of GO (in water) at 890 nm was used to determine the concentration of GO in the sample (please note that IR780 and SBMA-*g*-BSA do not have absorption at this wavelength). Subsequently, the absorption of IR/SBMA-BSA/GO at 808 nm, when dispersed in water/methanol (1:1 [v/v]), was acquired. Then, the determined concentration of GO and a standard curve of GO at 808 nm (in 1:1 [v/v] water/methanol) was used to determine the absorption of GO at 808 nm. Finally, the absorption of GO (at 808 nm) was subtracted to that of IR/SBMA-BSA/GO (at 808 nm), yielding the IR780 absorption (please note that SBMA-*g*-BSA does not absorb at this wavelength). Finally, a standard curve of IR780 at 808 nm (in 1:1 [v/v] water/methanol) was used to determine the concentration of IR780 in the IR/SBMA-BSA/GO sample [13,48].

The photothermal capacity of SBMA-BSA/GO and IR/SBMA-BSA/GO was determined by monitoring the temperature variations, using a thermocouple thermometer, upon irradiation of the nanostructures with NIR laser light for 10 min (808 nm, 1.7 W/cm^2) [15].

Evaluation of the cytocompatibility of SBMA-BSA/GO

The cytocompatibility of SBMA-BSA/GO toward MCF-7 cells and NHDF was evaluated through an MTS assay [53]. All cell lines were cultured in DMEM-F12 supplemented with 10% (v/v) of FBS and 1% (v/v) of penicillin/streptomycin in a humidified incubator (37°C, 5% CO_2). For this assay, MCF-7 cells and NHDF were seeded at a density of 1×10^4 cells/well in 96-well plates. After 24 h, the medium was removed, and cells were incubated with culture medium containing different doses of SBMA-BSA/GO for 24 or 48 h. Afterward, the nanomaterials were removed, and the cells were incubated with 120 µl of fresh medium containing MTS (20 µl) for 4 h in the dark (37°C, 5% CO_2). Then, the cells' viability was determined by analyzing the absorbance of the samples at 490 nm, using a microplate reader (xMark Microplate Spectrophotometer; Bio-Rad; Algés, Portugal). Negative (K^-) and positive (K^+) controls correspond to cells incubated solely with culture medium (without nanomaterials) and to cells treated with ethanol (70% [v/v]), respectively. Images of the cells after exposure to SBMA-BSA/GO were also acquired in an Olympus CX41 inverted optical microscope (10x objective; Olympus, Hamburg, Germany) equipped with an SP-500 UZ digital camera (Olympus).

10.2217/nnm-2020-0460

Evaluation of the phototherapeutic capacity of SBMA-BSA/GO & IR/SBMA-BSA/GO

The phototherapeutic effect mediated by SBMA-BSA/GO and IR/SBMA-BSA/GO was evaluated as previously described [13]. In brief, MCF-7 cells were seeded as described in 2.2.3. After 24 h, the medium was replaced by fresh medium containing different concentrations of SBMA-BSA/GO (40.0 and 65.0 μg/ml of GO equivalents) or IR/SBMA-BSA/GO (40.0/7.7 and 65.0/12.5 μg/ml of GO/IR780 equivalents). After 4 h, cells were irradiated with NIR light (808 nm, 1.7 W/cm^2, 10 min). Upon reaching 24 h of incubation, the nanomaterials were removed, and the cells' viability was evaluated as described in 2.2.3. Calcein-AM/PI staining was also performed (according to the manufactures' protocol) to visualize the live/dead cells after the different treatments by confocal laser scanning microscopy (Zeiss LSM 710 confocal microscope; Carl Zeiss AG, Oberkochen, Germany).

Statistical analysis

All data are presented as the mean ± standard deviation. One-way ANOVA with the Student–Newman–Keuls test was applied for the comparison of multiple groups. A p-value lower than 0.05 (*p <0.05) was considered statistically significant. For data analysis, GraphPad Prism v6.0 (Trial version, GraphPad Software, CA, USA) was used.

Results

Production & characterization of SBMA-BSA/GO & IR/SBMA-BSA/GO

For improving the colloidal stability and phototherapeutic capacity of GO, this nanomaterial was functionalized with SBMA-*g*-BSA and was loaded with IR780, respectively (Figure 1A). The SBMA-*g*-BSA was prepared as previously described elsewhere [48], by grafting SBMA into BSA using a Michael addition, and its synthesis was confirmed by FTIR (Supplementary Figure 1). The physicochemical properties of GO were also characterized (Supplementary Figures 2 & 3A), being in line with previous reports [53–56].

Then, GO was functionalized with SBMA-*g*-BSA by using a simple sonication process [13]. During this process, the GO sheets are exfoliated and the hydrophobic domains of SBMA-*g*-BSA adsorb into its aromatic surface, yielding SBMA-BSA/GO. The dynamic light scattering analysis demonstrated that the functionalization process of GO with SBMA-*g*-BSA improved its size distribution (Figure 1B). The nanosized dimensions of SBMA-BSA/GO were then confirmed by transmission electron microscopy (Supplementary Figure 3B).

Then, IR780 was loaded into the surface of SBMA-BSA/GO through noncovalent interactions (hydrophobic interactions and π-π stacking). The size distribution of IR/SBMA-BSA/GO was similar to that of SBMA-BSA/GO (Figure 1B). The zeta potentials of SBMA-BSA/GO (-29.6 ± 0.9 mV) and IR/SBMA-BSA/GO (-29.4 ± 1.2 mV) were also comparable. In contrast, nonfunctionalized GO presented a more negative surface charge (-43.8 ± 1.3 mV). The IR780 encapsulation efficiency in IR/SBMA-BSA/GO was of about 77 ± 14%. Furthermore, the IR/SBMA-BSA/GO was capable of adsorbing 0.192 ± 0.043 μg of IR780 per μg of GO.

Additionally, the stabilities of SBMA-BSA/GO and IR/SBMA-BSA/GO over time in cell culture medium (DMEM-F12 supplemented with 10% [v/v] of FBS) were assessed (Figure 1C). Both samples were capable of maintaining their size distribution over time (size variation <8% after 48 h of incubation). As control, the colloidal stability of GO (without any functionalization) and GO coated with BSA (non-SBMA functionalized) was also evaluated (Figure 1C). In this regard, GO and BSA/GO suffered an up to 63 and 31% increase in their size when incubated in cell culture medium, respectively.

Photothermal capacity of SBMA-BSA/GO & IR/SBMA-BSA/GO

To assess the ability of SBMA-BSA/GO and IR/SBMA-BSA/GO to interact with NIR light, their absorption spectra were acquired (Figure 1D). As expected, SBMA-BSA/GO exhibited a NIR absorption similar to that displayed by GO (Figure 1D). On the other hand, the spectrum of IR/SBMA-BSA/GO demonstrated an increased absorption in the 620–870 region, which is a characteristic feature of IR780 [48].

Then, the photothermal capacity of these nanomaterials was investigated (Figure 2 & Supplementary Figure 4). In general, SBMA-BSA/GO and IR/SBMA-BSA/GO produced a time- and concentration-dependent ΔT when irradiated with NIR light (Figure 2A & B). After 10 min of irradiation, SBMA-BSA/GO and IR/SBMA-BSA/GO could generate ΔT of about 14 and 28°C, respectively (at 65 μg/ml of GO equivalents) (Figure 2A & B). Furthermore, the response of water (control) to NIR light irradiation was meaningless (ΔT <2°C) (Figure 2A & B), which is justified by the weak interaction of 808 nm radiation with water [1].

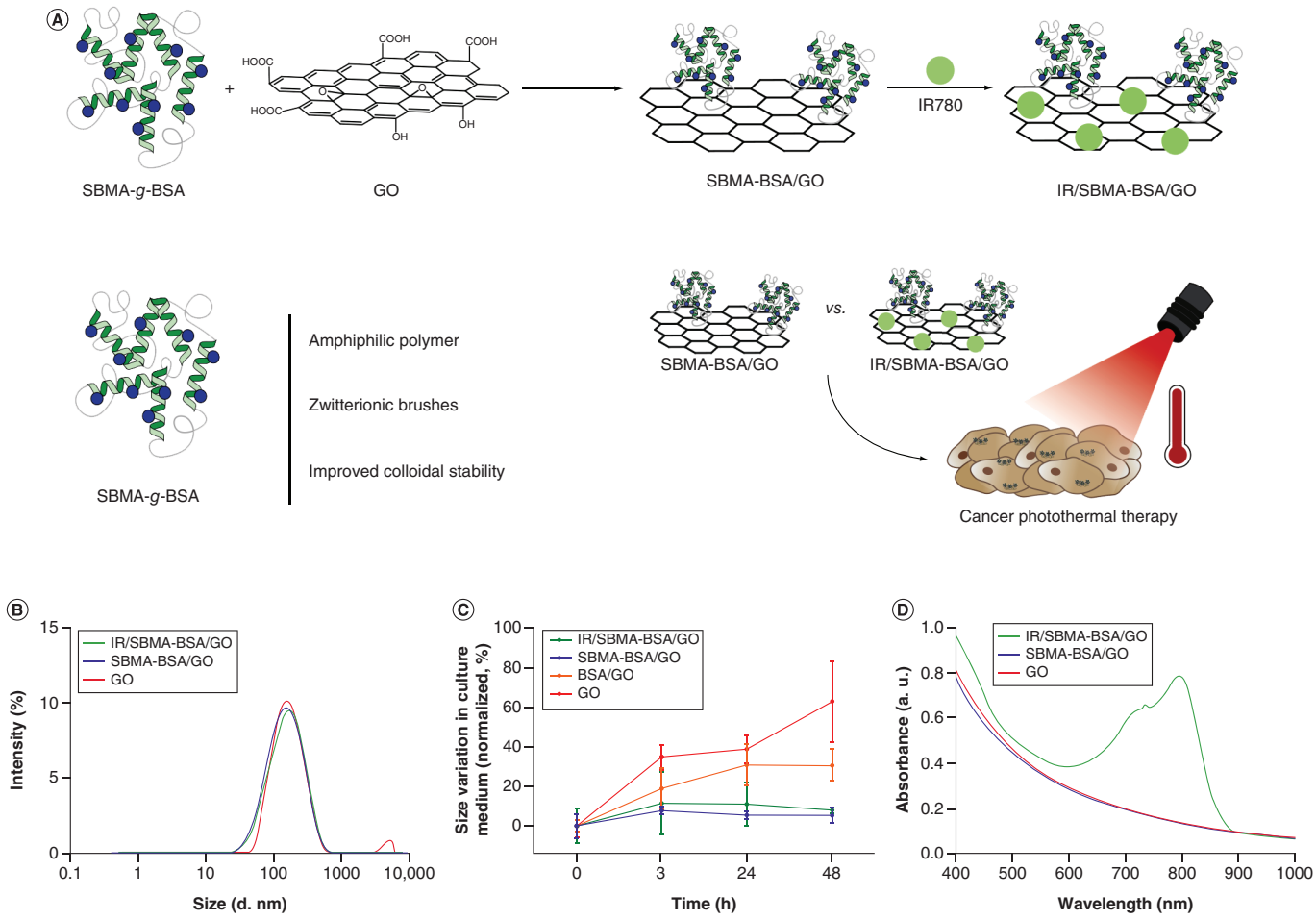

Figure 1. Preparation and physicochemical characterization of sulfobetaine methacrylate-grafted bovine serum albumin-functionalized graphene oxide and IR780-loaded sulfobetaine methacrylate-grafted bovine serum albumin-functionalized graphene oxide. Schematic representation of the application of SBMA-BSA/GO and IR/SBMA-BSA/GO in cancer photothermal therapy **(A)**. Dynamic light scattering size distribution of IR/SBMA-BSA/GO, SBMA-BSA/GO and GO **(B)**. Size variation of IR/SBMA-BSA/GO, SBMA-BSA/GO, BSA/GO and GO when dispersed in DMEM-F12 medium supplemented with 10% of fetal bovine serum (v/v). The values of each group were normalized using the respective initial size (t = 0 h). Each bar represents mean ± standard deviation (n = 3) **(C)**. Visible-near infrared absorption spectra of IR/SBMA-BSA/GO, SBMA-BSA/GO and GO **(D)**.
BSA: Bovine serum albumin; BSA/GO: BSA-functionalized GO; GO: Graphene oxide; IR/SBMA-BSA/GO: IR780-loaded SBMA-BSA/GO; SBMA: Sulfobetaine methacrylate; SBMA-BSA/GO: SBMA-*g*-BSA-functionalized GO; SBMA-g-BSA: SBMA-grafted BSA.

Evaluation of the cytocompatibility of SBMA-BSA/GO

Prior to determining the phototherapeutic capacity of the different SBMA-functionalized GO nanoformulations, the cytocompatibility of the SBMA-BSA/GO was investigated. For such, NHDF (healthy cell model) and MCF-7 cells (breast cancer cell model) were incubated with SBMA-BSA/GO during 24 and 48 h (Figure 3).

NHDF incubated with SBMA-BSA/GO did not have their viability affected in a meaningful way (cell viability >92%), even at a high SBMA-BSA/GO dose (75 µg/ml of GO equivalents) (Figure 3B). Furthermore, MCF-7 cells incubated with SBMA-BSA/GO also revealed a high cell viability (>93%) (Figure 3A). Moreover, SBMA-BSA/GO did not cause any detectable changes in the morphology of both cell lines (Supplementary Figure 5).

Evaluation of the PTT mediated by SBMA-BSA/GO & IR/SBMA-BSA/GO

Then, the phototherapeutic capacities of SBMA-BSA/GO and IR/SBMA-BSA/GO toward breast cancer cells were investigated. For this purpose, MCF-7 cells were incubated with the nanomaterials and then were exposed to NIR light (808 nm, 1.7 W/cm^2, 10 min) (Figure 4A).

10.2217/nnm-2020-0460

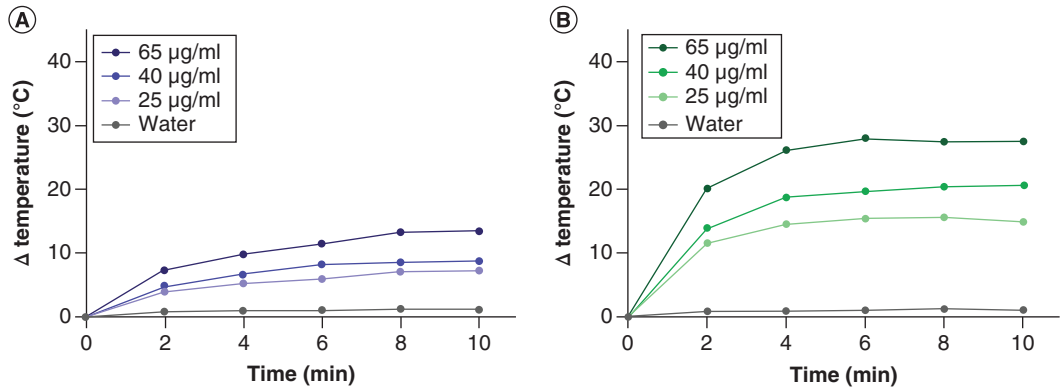

Figure 2. Characterization of the photothermal capacity of sulfobetaine methacrylate-grafted bovine serum albumin-functionalized graphene oxide and IR780-loaded sulfobetaine methacrylate-grafted bovine serum albumin-functionalized graphene oxide. Temperature variation curves of sulfobetaine methacrylate-grafted bovine serum albumin-functionalized graphene oxide (SBMA-BSA/GO) **(A)** and IR780-loaded SBMA-BSA/GO **(B)** at different concentrations (of GO equivalents) during 10 min of near infrared irradiation (808 nm, 1.7 W/cm^2).

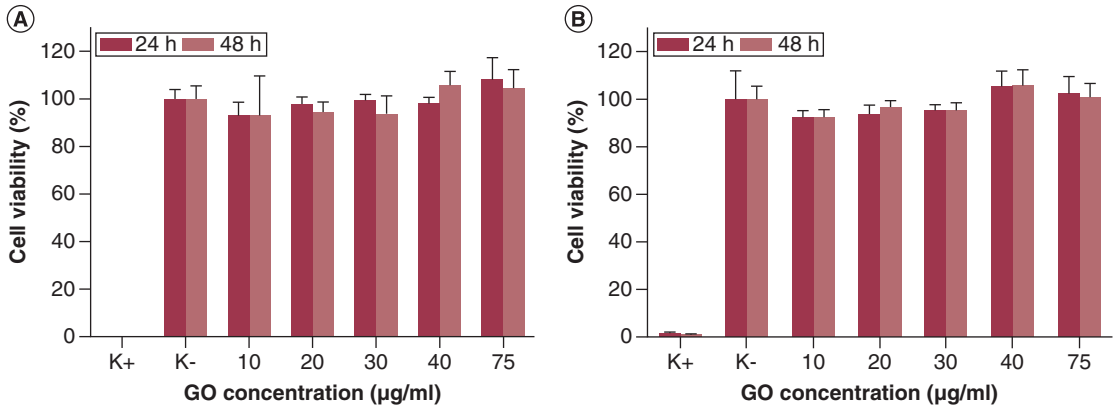

Figure 3. Evaluation of the cytocompatibility profile of sulfobetaine methacrylate-grafted bovine serum albumin-functionalized graphene oxide. Cell viability of MCF-7 cells **(A)** and normal human dermal fibroblast **(B)** incubated with sulfobetaine methacrylate-grafted bovine serum albumin-functionalized GO at different concentrations (of GO equivalents) during 24 and 48 h. Data represent mean ± standard deviation, n = 5. K^- and K^+ represent the negative and positive controls, respectively.

As expected, MCF-7 cells solely incubated with SBMA-BSA/GO or only exposed to NIR light did not show a decrease in their viability (Figure 4B). Such result is in agreement with the good cytocompatibility displayed by SBMA-BSA/GO (Figure 3A) and with the insignificant off-target heating induced by water when exposed to NIR light (Figure 2). Surprisingly, the combination of NIR light with SBMA-BSA/GO did not reduce the viability of the cancer cells, even at a relatively high nanomaterial's dose (65 µg/ml of GO equivalents) (Figure 4B).

On the other hand, the two tested doses of nonirradiated IR/SBMA-BSA/GO (40.0/7.7 and 65.0/12.5 µg/ml of GO/IR780 equivalents) induced a similar reduction on cancer cells' viability to about 67% (Figure 4B). In turn, upon irradiation with NIR light, the IR/SBMA-BSA/GO could greatly decrease the viability of MCF-7 cells (Figure 4B). At the highest concentration tested (65.0/12.5 µg/ml of GO/IR780 equivalents), the combination of IR/SBMA-BSA/GO with NIR light reduced the cancer cells' viability to <2% (Figure 4B). These results were further corroborated by confocal laser scanning microscopy images of MCF-7 cells stained with Calcein-AM (labels viable cells) and PI (labels dead cells) (Figure 4C & D).

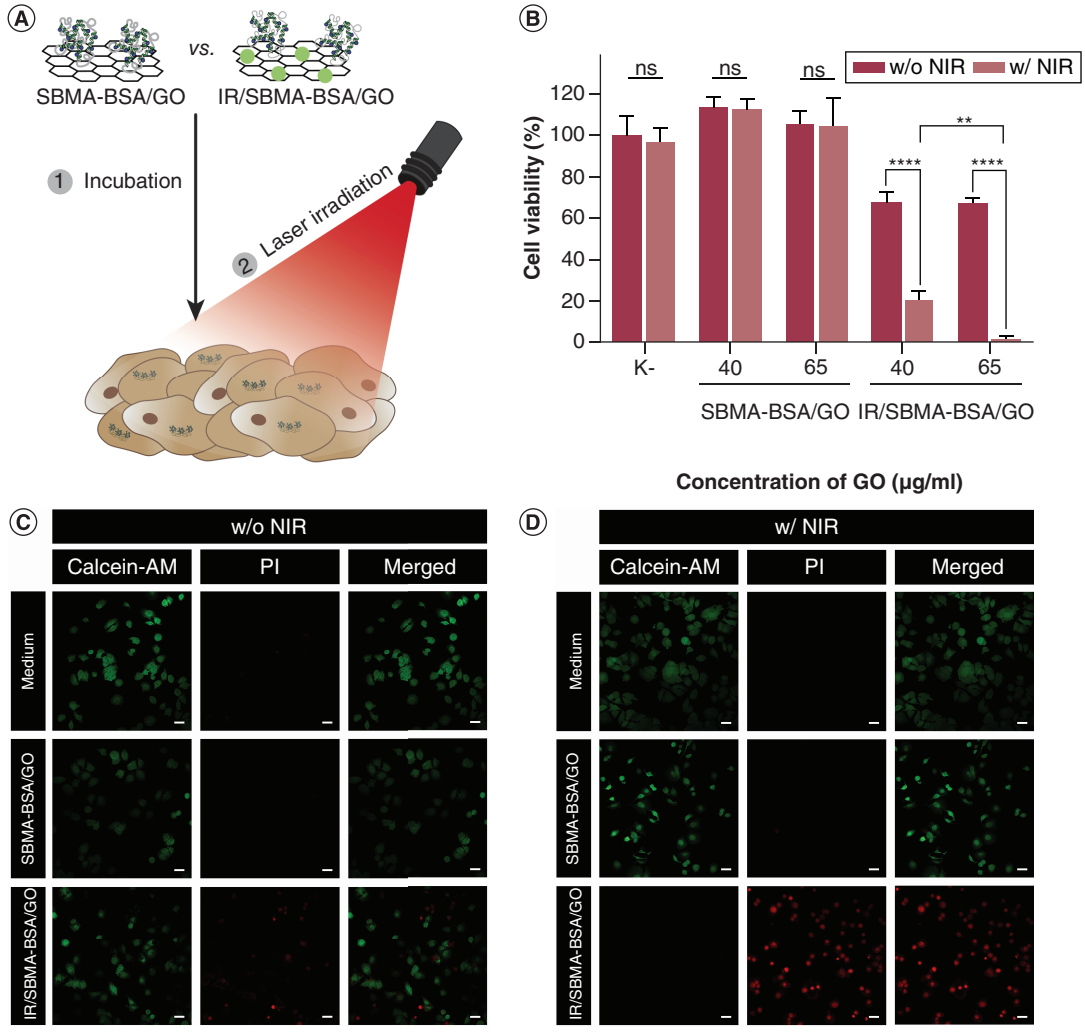

Figure 4. Evaluation of the phototherapeutic capacity of sulfobetaine methacrylate-grafted bovine serum albumin-functionalized graphene oxide and IR780-loaded sulfobetaine methacrylate-grafted bovine serum albumin-functionalized graphene oxide. Schematic representation of the photothermal therapy mediated by SBMA-BSA/GO and IR/SBMA-BSA/GO against MCF-7 cells **(A)**. Therapeutic effect mediated by SBMA-BSA/GO and IR/SBMA-BSA/GO against MCF-7 cells w/o NIR and w/ NIR laser irradiation (808 nm, 1.7 W/cm^2, 10 min) **(B)**. K^- w/o NIR represents the negative control. K^- w/ NIR represents cells solely exposed to NIR light. Data represents mean ± standard deviation, n = 5 (**p <0.01; ****p <0.0001). Confocal laser scanning microscopy images of MCF-7 cells stained with Calcein-AM/PI after incubation with SBMA-BSA/GO (65.0 μg/ml of GO equivalents) or IR/SBMA-BSA/GO (65.0/12.5 μg/ml of GO/IR780 equivalents) w/o NIR **(C)** or w/ NIR laser irradiation (808 nm, 1.7 W/cm^2, 10 min) **(D)**. The control for live cells (medium w/o NIR) was also performed. Cells incubated with medium and solely exposed to NIR light (medium w/ NIR) were also analyzed. Green channel: Calcein-AM; red channel: PI. Scale bars correspond to 50 μm.
GO: Graphene oxide; IR/SBMA-BSA/GO: IR780-loaded SBMA-BSA/GO; NIR: Near infrared; ns: Nonsignificant; PI: Propidium iodide; SBMA-BSA/GO: Sulfobetaine methacrylate-grafted bovine serum albumin-functionalized GO; w/: With; w/o: Without.

Discussion

The NIR absorption of GO nanomaterials has propelled their investigation for cancer PTT. However, as-synthesized GO presents poor colloidal stability and subpar photothermal capacity, hindering its full therapeutic potential. To address these limitations, in this work GO was coated with SBMA-*g*-BSA and was loaded with IR780.

The functionalization process of GO with SBMA-*g*-BSA improved its size distribution (Figure 1B). In fact, SBMA-BSA/GO displayed nanometric dimensions (Supplementary Figure 3B) that are within the size distribution considered as optimal for passive tumor accumulation [1,57]. Then, IR780 was loaded into SBMA-BSA/GO. Im-

10.2217/nnm-2020-0460

portantly, the loading of this phototherapeutic agent did not significantly impact the nanomaterials' size (Figure 1B & Supplementary Figure 3C).

The SBMA-BSA/GO and IR/SBMA-BSA/GO presented a similar surface charge ($\zeta \approx$ -29 mV) that contrasts with that presented by GO (ζ = -43.8 $\pm$ 1.3 mV). Such data suggest that the SBMA-*g*-BSA-based coating can attenuate part of the negative surface charge displayed by the GO nanostructures. The encapsulation efficiency of IR780 in the IR/SBMA-BSA/GO was higher than that displayed by other GO-based nanomaterials [58,59]. The high loading capacity of IR/SBMA-BSA/GO is an inherent property of GO-based nanomaterials [13,60], and also results from the fact that GO nanosheets without IR780 are removed during the nanomaterials' purification phase (centrifugation step).

When dispersed in cell culture medium, both SBMA-BSA/GO and IR/SBMA-BSA/GO revealed excellent colloidal stability since their size was not severely affected over time (Figure 1C). In the same conditions, the size of BSA/GO and GO increased by up to 31 and 63%, respectively (Figure 1C). These findings reveal that the improved colloidal stability of SBMA-BSA/GO and IR/SBMA-BSA/GO results from the SBMA functionalization. In fact, it has been previously demonstrated that the grafting of SBMA into the surface of polymeric nanoparticles also enhances their colloidal stability [48]. Furthermore, tri-block copolymers based on SBMA-poly(ethylenimine)-poly(maleic anhydride-*alt*-1-octadecene) conjugates were recently reported to be capable of improving the colloidal stability of GO [17]. In this context, the SBMA-*g*-BSA coating employed in this work can also endow GO with an optimal colloidal stability and may be more advantageous due to the good *in vivo* biocompatibility and biodegradability of BSA [61,62]. Moreover, the coating of nanostructures with SBMA has been reported to decrease protein adsorption on the nanostructures' surface, hence increasing their stability during circulation and prompting their tumor accumulation [63–65].

After confirming that the SBMA-BSA/GO and IR/SBMA-BSA/GO presented suitable physicochemical properties for application in cancer therapy, we investigated their photothermal capacity. Upon NIR laser irradiation, both formulations produced ΔT that can potentially induce irreversible damage to cancer cells (e.g., protein denaturation, membrane collapse and enzymatic/mitochondrial dysfunctions), ultimately leading to their death by necrosis (Figure 2 & Supplementary Figure 4) [1,66].

The IR/SBMA-BSA/GO could produce an up to two-times higher photoinduced heat than SBMA-BSA/GO (Figure 2A & B). The higher photothermal capacity of IR/SBMA-BSA/GO is related to its 5.6-times higher absorption at 808 nm when compared with SBMA-BSA/GO (Figure 1D). For instance, Justin and coworkers prepared reduced GO–iron oxide-based nanohybrids that could produce ΔT of 13°C after NIR laser irradiation (50 μg/ml; 808 nm, 2.5 W/cm^2, 10 min) [67]. Herein, the IR/SBMA-BSA/GO generated a photoinduced heat of 21°C (ΔT) using a lower concentration of NIR-responsive agents and a weaker radiation intensity (40.0/7.7 μg/ml of GO/IR780 equivalents; 808 nm, 1.7 W/cm^2, 10 min). In this way, the incorporation of IR780 in SBMA-BSA/GO is a straightforward nonlaborious process for improving the photothermal capacity of this nanomaterial.

When incubated on NHDF and MCF-7 cells, the SBMA-BSA/GO did not affect meaningfully the cells' viability (Figure 3) neither induced appreciable changes on cells' morphology (Supplementary Figure 5). These results are in line with the excellent cytocompatibility displayed by SBMA-functionalized nanomaterials and by BSA-based nanoformulations [49,61,62,68]. Surprisingly, MCF-7 cells treated with SBMA-BSA/GO plus NIR light also remained highly viable (Figure 4B & D). These data further confirm the importance of improving GO photothermal capacity in order to achieve an appropriate therapeutic effect. On the other hand, nonirradiated IR/SBMA-BSA/GO could decrease the viability of cancer cells to about 67% (Figure 4B & C). This effect may result from the IR780 propensity to accumulate on the mitochondria of MCF-7 cells, leading to a slight cytotoxic effect [69,70]. In stark contrast, the combined action of IR/SBMA-BSA/GO and NIR light induced the ablation of cancer cells (cell viability <2%) (Figure 4B & D). Considering that the interaction of SBMA-BSA/GO with NIR light did not cause any cytotoxicity, these findings confirm that the encapsulation of IR780 in the SBMA-functionalized GO can be pursued to improve its phototherapeutic capacity.

For instance, Sun *et al.* grew gold nanorods on the surface of GO materials, demonstrating that the PTT mediated by these hybrid structures could reduce cancer cells' viability to about 17% (808 nm, 0.8 W/cm^2, 10 min; 50 μg/ml of Au) [43]. On the other hand, Wu *et al.* performed the growth of CuS nanoparticles on the surface of GO nanosheets, verifying that this nanohybrid could induce a reduction on breast cancer cells' viability to 45% upon NIR laser irradiation (940 nm, 4 W/cm^2, 5 min; 50 μg/ml of nanohybrids) [71]. Herein, IR/SBMA-BSA/GO were prepared by just encapsulating IR780 in SBMA-BSA/GO, rendering a hybrid nanosystem whose photothermal effect diminished cancer cells' viability to 2% (808 nm, 1.7 W/cm^2, 10 min; 65.0/12.5 μg/ml

of GO/IR780 equivalents). In this way, IR/SBMA-BSA/GO is a promising agent for application in the PTT of breast cancer cells.

Conclusion

In this work, GO was functionalized with SBMA-*g*-BSA and loaded with IR780, for the first time, in order to improve its colloidal stability and photothermal capacity. The SBMA-BSA/GO and IR/SBMA-BSA/GO were produced using a simple sonication method and presented an adequate size distribution. When in contact with biologically relevant media, the size of SBMA-BSA/GO and IR/SBMA-BSA/GO only increased by 8% after 48 h, revealing an excellent colloidal stability. In the same condition, the GO and BSA/GO suffered a 63 and 31% increase in their size, respectively. By loading IR780 into SBMA-BSA/GO, its NIR absorption increased by 5.6-fold. In this way, the IR/SBMA-BSA/GO could produce an up to two-times higher photoinduced heat than SBMA-BSA/GO. In *in vitro* studies, the combination of NIR light with SBMA-BSA/GO did not induce any photocytotoxicity on breast cancer cells. In stark contrast, the interaction of IR/SBMA-BSA/GO with NIR light was able to induce the ablation of cancer cells (cell viability <2%). Overall, IR/SBMA-BSA/GO displays a greatly improved colloidal stability and phototherapeutic capacity, being a promising nanohybrid for application in the PTT of breast cancer cells. In the future, *in vivo* assays will be crucial to fully depict the phototherapeutic capacity of IR/SBMA-BSA/GO.

Future perspective

GO derivatives have been functionalized with PEG-based coatings in order to improve their colloidal stability. On the other hand, this nanomaterial has also been reduced using hydrazine hydrate for improving its photothermal capacity. These two strategies present critical limitations since PEG-based coatings can be immunogenic and the hydrazine hydrate reduction hinders the materials' biocompatibility. In the future years, the investigation of novel coatings that are not prone to suffer from the ABC phenomenon, and their use to functionalize GO derivatives will be crucial to accelerate the nanomaterials' translation. In turn, the photothermal capacity of this nanomaterial may be enhanced by loading different NIR-responsive molecules on its lattice or by exploring environmentally friendly and nonhazardous reduction methods. The phototherapeutic capacity of GO may also be explored in conjugation with other therapeutic modalities (e.g., immunotherapy), opening a venue for a revolutionized cancer therapy.

Summary points

- The sulfobetaine methacrylate (SBMA)-functionalized graphene oxide (GO) derivatives displayed improved colloidal stability in biologically relevant media (size variation <8%).
- The loading of IR780 into SBMA-grafted bovine serum albumin (BSA)-functionalized GO (SBMA-BSA/GO) increased the nanomaterials' near infrared (NIR) absorption by 5.6-fold.
- The enhanced NIR absorption of IR780-loaded SBMA-BSA/GO enabled the production of an up to two-times higher photoinduced heat.
- SBMA-BSA/GO was cytocompatible toward both healthy and breast cancer cells.
- SBMA-BSA/GO in combination with NIR light did not induce any photocytotoxicity on breast cancer cells.
- IR780-loaded SBMA-BSA/GO in combination with NIR light caused the ablation of breast cancer cells.

Supplementary data

To view the supplementary data that accompany this paper please visit the journal website at: www.futuremedicine.com/doi/suppl/10.2217/nnm-2020-0460

Author contributions

D de Melo-Diogo contributed to the conceptualization of the study. BL Melo, R Lima-Sousa, CG Alves, P Ferreira, AF Moreira and D de Melo-Diogo contributed to the investigation of the study. BL Melo participated in the formal analysis of the study. BL Melo was involved in writing the original draft of this study. R Lima-Sousa, IJ Correia and D de Melo-Diogo supervised the study, and contributed to the review and editing of the written draft. IJ Correia contributed to the project administration and funding acquisition.

Financial & competing interests disclosure

This work was financed by the Foundation for Science and Technology (FCT), through funds from the State Budget, and by the European Regional Development Fund (ERDF), under the Portugal 2020 Program, through the Regional Operational Program of the Center (Centro2020), through the Project with the reference UIDB/00709/2020. The funding from CENTRO-01-0145-FEDER-028989 and POCI-01-0145-FEDER-031462 are also acknowledged. D de Melo-Diogo acknowledges CENTRO-01-0145-FEDER-028989 for the funding given on the form of a research contract. CG Alves and R Lima-Sousa acknowledge funding from individual PhD fellowships from FCT (SFRH/BD/145386/2019 and SFRH/BD/144922/2019). The authors have no other relevant affiliations or financial involvement with any organization or entity with a financial interest in or financial conflict with the subject matter or materials discussed in the manuscript apart from those disclosed.

No writing assistance was utilized in the production of this manuscript.

References

Papers of special note have been highlighted as: • of interest; •• of considerable interest

1. de Melo-Diogo D, Pais-Silva C, Dias DR, Moreira AF, Correia IJ. Strategies to improve cancer photothermal therapy mediated by nanomaterials. *Adv. Healthcare Mater.* 6, 1700073 (2017).
2. Liu Y, Bhattarai P, Dai Z, Chen X. Photothermal therapy and photoacoustic imaging via nanotheranostics in fighting cancer. *Chem. Soc. Rev.* 48, 2053–2108 (2019).
3. Magro M, Venerando A, Macone A, Canettieri GAgostinelli E, Vianello F. Nanotechnology-based strategies to develop new anticancer therapies. *Biomolecules* 10, 735 (2020).
4. Siddique S, Chow JC. Application of nanomaterials in biomedical imaging and cancer therapy. *Nanomaterials* 10, 1700 (2020).
5. Gunduz N, Ceylan H, Guler MO, Tekinay AB. Intracellular accumulation of gold nanoparticles leads to inhibition of macropinocytosis to reduce the endoplasmic reticulum stress. *Sci. Rep.* 7, 40493 (2017).
6. Jacinto TA, Rodrigues CF, Moreira AF *et al.* Hyaluronic acid and vitamin E polyethylene glycol succinate functionalized gold-core silica shell nanorods for cancer targeted photothermal therapy. *Colloids Surf., B* 188, 110778 (2020).
7. Guo L, Yan DD, Yang D, Li Y, Wang X, Zalewski O *et al.* Combinatorial photothermal and immuno cancer therapy using chitosan-coated hollow copper sulfide nanoparticles. *ACS Nano* 8, 5670–5681 (2014).
8. Liu G, Gao N, Zhou Y, Nie J, Cheng W, Luo M *et al.* Polydopamine-based "four-in-one" versatile nanoplatforms for targeted dual chemo and photothermal synergistic cancer therapy. *Pharmaceutics* 11, 507 (2019).
9. de Melo-Diogo D, Lima-Sousa R, Alves CG, Costa EC, Louro RO, Correia IJ. Functionalization of graphene family nanomaterials for application in cancer therapy. *Colloids Surf., B* 171, 260–275 (2018).

•• **Summarizes the different functionalizations that enable the application of graphene-based nanomaterials in cancer therapy.**

10. Yang K, Wan J, Zhang S, Tian BZhang Y, Liu Z. The influence of surface chemistry and size of nanoscale graphene oxide on photothermal therapy of cancer using ultra-low laser power. *Biomaterials* 33, 2206–2214 (2012).
11. Ma X, Tao H, Yang K, Feng L, Cheng L, Shi X *et al.* A functionalized graphene oxide-iron oxide nanocomposite for magnetically targeted drug delivery, photothermal therapy, and magnetic resonance imaging. *Nano Res.* 5, 199–212 (2012).
12. Qiu Z, Hu J, Li Z, Yang X, Hu J, You Q *et al.* Graphene oxide-based nanocomposite enabled highly efficient targeted synergistic therapy for colorectal cancer. *Colloids Surf., A* 593, 124585 (2020).
13. de Melo-Diogo D, Costa EC, Alves CG, Lima-Sousa R, Ferreira P, Louro RO *et al.* POxylated graphene oxide nanomaterials for combination chemo-phototherapy of breast cancer cells. *Eur. J. Pharm. Biopharm.* 131, 162–169 (2018).
14. Wang Y, Wang H, Liu D, Song SWang X, Zhang H. Graphene oxide covalently grafted upconversion nanoparticles for combined NIR mediated imaging and photothermal/photodynamic cancer therapy. *Biomaterials* 34, 7715–7724 (2013).
15. Lima-Sousa R, de Melo-Diogo D, Alves CG, Cabral CSD, Miguel SP, Mendonça AG *et al.* Injectable *in situ* forming thermo-responsive graphene based hydrogels for cancer chemo-photothermal therapy and NIR light-enhanced antibacterial applications. *Mater. Sci. Eng.* 117, 111294 (2020).
16. Strangman G, Boas DA, Sutton JP. Non-invasive neuroimaging using near-infrared light. *Biol. Psychiatry* 52, 679–693 (2002).
17. Leitão MM, Alves CG, de Melo-Diogo D, Lima-Sousa R, Moreira AF, Correia IJ. Sulfobetaine methacrylate-functionalized graphene oxide-IR780 nanohybrids aimed at improving breast cancer phototherapy. *RSC Adv.* 10, 38621–38630 (2020).
18. Qin XC, Guo ZY, Liu ZM, Zhang W, Wan MM, Yang BW. Folic acid-conjugated graphene oxide for cancer targeted chemo-photothermal therapy. *J. Photochem. Photobiol. B* 120, 156–162 (2013).
19. Nakielski P, Pawłowska S, Rinoldi C, Ziai Y, De Sio L, Urbanek O *et al.* Multifunctional platform based on electrospun nanofibers and plasmonic hydrogel: a smart nanostructured pillow for near-infrared light-driven biomedical applications. *ACS Appl. Mater. Interfaces* 12, 54328–54342 (2020).

20. Bai JLiu Y, Jiang X. Multifunctional PEG-GO/CuS nanocomposites for near-infrared chemo-photothermal therapy. *Biomaterials* 35, 5805–5813 (2014).
21. De Sio L, Ding B, Focsan M, Kogermann K, Pascoal-Faria P, Petronella F *et al.* Personalized reusable face masks with smart nano-assisted destruction of pathogens for COVID-19: a visionary road. *Chem. Eur. J.* (2020) (In Press).
22. Gudarzi MM. Colloidal stability of graphene oxide: aggregation in two dimensions. *Langmuir* 32, 5058–5068 (2016).
23. Liu Z, Robinson JTSun X, Dai H. PEGylated nanographene oxide for delivery of water-insoluble cancer drugs. *J. Am. Chem. Soc.* 130, 10876–10877 (2008).
24. Tian B, Wang C, Zhang SFeng L, Liu Z. Photothermally enhanced photodynamic therapy delivered by nano-graphene oxide. *ACS Nano* 5, 7000–7009 (2011).
25. Luo N, Weber JK, Wang S, Luan B, Yue H, Xi X *et al.* PEGylated graphene oxide elicits strong immunological responses despite surface passivation. *Nat. Commun.* 8, 1–10 (2017).
- **Demonstrates that PEGylated graphene oxide derivatives suffer from the accelerated blood clearance phenomenon.**
26. Suzuki T, Ichihara M, Hyodo K, Yamamoto E, Ishida T, Kiwada H *et al.* Accelerated blood clearance of PEGylated liposomes containing doxorubicin upon repeated administration to dogs. *Int. J. Pharm.* 436, 636–643 (2012).
27. Ishida T, Harada M, Wang XY, Ichihara MIrimura K, Kiwada H. Accelerated blood clearance of PEGylated liposomes following preceding liposome injection: effects of lipid dose and PEG surface-density and chain length of the first-dose liposomes. *J. Control. Release* 105, 305–317 (2005).
28. Ishida T, Kiwada H. Accelerated blood clearance (ABC) phenomenon upon repeated injection of PEGylated liposomes. *Int. J. Pharm.* 354, 56–62 (2008).
29. Laverman P, Carstens MG, Boerman OC, Dams ETM, Oyen WJ, van Rooijen N *et al.* Factors affecting the accelerated blood clearance of polyethylene glycol-liposomes upon repeated injection. *J. Pharmacol. Exp. Ther.* 298, 607–612 (2001).
30. Yin T, Liu J, Zhao Z, Zhao Y, Dong L, Yang M *et al.* Redox sensitive hyaluronic acid-decorated graphene oxide for photothermally controlled tumor-cytoplasm-selective rapid drug delivery. *Adv. Funct. Mater.* 27, 1604620 (2017).
31. Li Q, Hong LLi H, Liu C. Graphene oxide-fullerene C60 (GO-C60) hybrid for photodynamic and photothermal therapy triggered by near-infrared light. *Biosens. Bioelectron.* 89, 477–482 (2017).
32. Yang K, Zhang S, Zhang G, Sun X, Lee S-T, Liu Z. Graphene in mice: ultrahigh *in vivo* tumor uptake and efficient photothermal therapy. *Nano Lett.* 10, 3318–3323 (2010).
33. Lim JH, Kim DE, Kim E-J, Ahrberg CD, Chung BG. Functional graphene oxide-based nanosheets for photothermal therapy. *Macromol. Res.* 26, 557–565 (2018).
34. Hu Y, Sun D, Ding JChen L, Chen X. Decorated reduced graphene oxide for photo-chemotherapy. *J. Mater. Chem. B* 4, 929–937 (2016).
35. Robinson JT, Tabakman SM, Liang Y, Wang H, Sanchez Casalongue H, Vinh D *et al.* Ultrasmall reduced graphene oxide with high near-infrared absorbance for photothermal therapy. *J. Am. Chem. Soc.* 133, 6825–6831 (2011).
36. Dervin S, Murphy J, Aviles R, Pillai SC, Garvey M. An *in vitro* cytotoxicity assessment of graphene nanosheets on alveolar cells. *Appl. Surf. Sci.* 434, 1274–1284 (2018).
37. Akhavan OGhaderi E, Emamy H. Nontoxic concentrations of PEGylated graphene nanoribbons for selective cancer cell imaging and photothermal therapy. *J. Mater. Chem.* 22, 20626–20633 (2012).
38. Akhavan O, Ghaderi E. Graphene nanomesh promises extremely efficient *in vivo* photothermal therapy. *Small* 9, 3593–3601 (2013).
39. Akhavan O. Bacteriorhodopsin as a superior substitute for hydrazine in chemical reduction of single-layer graphene oxide sheets. *Carbon* 81, 158–166 (2015).
40. Abdolahad M, Janmaleki M, Mohajerzadeh SAkhavan O, Abbasi S. Polyphenols attached graphene nanosheets for high efficiency NIR mediated photodestruction of cancer cells. *Mater. Sci. Eng.* 33, 1498–1505 (2013).
41. Akhavan O, Ghaderi E, Aghayee SFereydooni Y, Talebi A. The use of a glucose-reduced graphene oxide suspension for photothermal cancer therapy. *J. Mater. Chem.* 22, 13773–13781 (2012).
42. Hatamie S, Akhavan O, Sadrnezhaad SK, Ahadian MM, Shirolkar MM, Wang HQ. Curcumin-reduced graphene oxide sheets and their effects on human breast cancer cells. *Mater. Sci. Eng.* 55, 482–489 (2015).
43. Sun B, Wu J, Cui S, Zhu H, An W, Fu Q *et al. In situ* synthesis of graphene oxide/gold nanorods theranostic hybrids for efficient tumor computed tomography imaging and photothermal therapy. *Nano Res.* 10, 37–48 (2017).
44. Akhavan O, Meidanchi AGhaderi E, Khoei S. Zinc ferrite spinel-graphene in magneto-photothermal therapy of cancer. *J. Mater. Chem. B* 2, 3306–3314 (2014).
45. Shirshahi V, Hatamie S, Tabatabaei SNSalimi M, Saber R. Enhanced thermal stability and biocompatibility of gold nanorods by graphene oxide. *Plasmonics* 13, 1585–1594 (2018).
46. Gonzalez-Rodriguez RCampbell E, Naumov A. Multifunctional graphene oxide/iron oxide nanoparticles for magnetic targeted drug delivery dual magnetic resonance/fluorescence imaging and cancer sensing. *PLoS ONE* 14, e0217072 (2019).

47. Han L, Hao Y-N, Wei X, Chen X-WShu Y, Wang J-H. Hollow copper sulfide nanosphere–doxorubicin/graphene oxide core–shell nanocomposite for photothermo-chemotherapy. *ACS Biomater. Sci. Eng.* 3, 3230–3235 (2017).

48. Alves CG, de Melo-Diogo D, Lima-Sousa R, Correia IJ. IR780 loaded sulfobetaine methacrylate-functionalized albumin nanoparticles aimed for enhanced breast cancer phototherapy. *Int. J. Pharm.* 582, 119346 (2020).

• **Describes the advantages of grafting sulfobetaine methacrylate into bovine serum albumin for cancer-related applications.**

49. Almutary AG, Sanderson BJAlhalili Z, Ellis AV. Toxicity of thiolated silica nanoparticles modified with sulfobetaine methacrylate for potential use in chemotherapy drug conjugation. *J. Appl. Pharm. Sci.* 7, 001–009 (2017).

50. Men Y, Peng S, Yang P, Jiang Q, Zhang Y, Shen B *et al.* Biodegradable zwitterionic nanogels with long circulation for antitumor drug delivery. *ACS Appl. Mater. Interfaces* 10, 23509–23521 (2018).

51. Mó I, Alves CG, de Melo-Diogo D, Lima-Sousa R, Correia IJ. Assessing the combinatorial chemo-photothermal therapy mediated by sulfobetaine methacrylate-functionalized nanoparticles in 2D and 3D *in vitro* cancer models. *Biotechnol. J.* 15, 2000219 (2020).

52. Leitão MM, de Melo-Diogo D, Alves CG, Lima-Sousa R, Correia IJ. Prototypic heptamethine cyanine incorporating nanomaterials for cancer phototheragnostic. *Adv. Healthcare Mater.* 9, 1901665 (2020).

•• **Summarizes the application of nanomaterials incorporating prototypic heptamethine cyanines in cancer photothermal therapy.**

53. Cabral CS, Miguel SP, de Melo-Diogo D, Louro RO, Correia IJ. Green reduced graphene oxide functionalized 3D printed scaffolds for bone tissue regeneration. *Carbon* 146, 513–523 (2019).

54. Marcano DC, Kosynkin DV, Berlin JM, Sinitskii A, Sun Z, Slesarev A *et al.* Improved synthesis of graphene oxide. *ACS Nano* 4, 4806–4814 (2010).

55. de Melo-Diogo D, Pais-Silva C, Costa EC, Louro RO, Correia IJ. D-α-tocopheryl polyethylene glycol 1000 succinate functionalized nanographene oxide for cancer therapy. *Nanomedicine* 12, 443–456 (2017).

56. Díez-Pascual AM, Sainz-Urruela C, Vallés C, Vera-López S, San Andrés MP. Tailorable synthesis of highly oxidized graphene oxides via an environmentally-friendly electrochemical process. *Nanomaterials* 10, 239 (2020).

57. Blanco EShen H, Ferrari M. Principles of nanoparticle design for overcoming biological barriers to drug delivery. *Nat. Biotechnol.* 33, 941 (2015).

58. Mahajan CR, Joshi LB, Varma U, Naik JB, Chaudhari VR, Mishra S. Sustainable drug delivery of famotidine using chitosan-functionalized graphene oxide as nanocarrier. *Glob. Chang.* 3, 1900002 (2019).

59. Chauhan DS, Kumawat MK, Prasad R, Reddy PK, Dhanka M, Mishra SK *et al.* Plasmonic carbon nanohybrids for repetitive and highly localized photothermal cancer therapy. *Colloids Surf., B* 172, 430–439 (2018).

60. Yang X, Wang Y, Huang X, Ma Y, Huang Y, Yang R *et al.* Multi-functionalized graphene oxide based anticancer drug-carrier with dual-targeting function and pH-sensitivity. *J. Mater. Chem.* 21, 3448–3454 (2011).

61. An F-F, Zhang X-H. Strategies for preparing albumin-based nanoparticles for multifunctional bioimaging and drug delivery. *Theranostics* 7, 3667 (2017).

62. Lin T, Zhao P, Jiang Y, Tang Y, Jin H, Pan Z *et al.* Blood–brain barrier-penetrating albumin nanoparticles for biomimetic drug delivery via albumin-binding protein pathways for antiglioma therapy. *ACS Nano* 10, 9999–10012 (2016).

63. Wu J, He C, He H, Cheng C, Zhu J, Xiao Z *et al.* Importance of zwitterionic incorporation into polymethacrylate-based hydrogels for simultaneously improving optical transparency, oxygen permeability, and antifouling properties. *J. Mater. Chem. B* 5, 4595–4606 (2017).

64. Chang Y, Chen SZhang Z, Jiang S. Highly protein-resistant coatings from well-defined diblock copolymers containing sulfobetaines. *Langmuir* 22, 2222–2226 (2006).

65. Peng S, Ouyang B, Men Y, Du Y, Cao Y, Xie R *et al.* Biodegradable zwitterionic polymer membrane coating endowing nanoparticles with ultra-long circulation and enhanced tumor photothermal therapy. *Biomaterials* 231, 119680 (2020).

66. Chu KF, Dupuy DE. Thermal ablation of tumours: biological mechanisms and advances in therapy. *Nat. Rev. Cancer* 14, 199–208 (2014).

67. Justin R, Tao K, Román S, Chen D, Xu Y, Geng X *et al.* Photoluminescent and superparamagnetic reduced graphene oxide–iron oxide quantum dots for dual-modality imaging, drug delivery and photothermal therapy. *Carbon* 97, 54–70 (2016).

68. Zhang M, Shen W, Xiong Q, Wang H, Zhou Z, Chen W *et al.* Thermo-responsiveness and biocompatibility of star-shaped poly [2-(dimethylamino) ethyl methacrylate]-b-poly (sulfobetaine methacrylate) grafted on a β-cyclodextrin core. *RSC Adv.* 5, 28133–28140 (2015).

69. Wang Y, Liu T, Zhang E, Luo STan X, Shi C. Preferential accumulation of the near infrared heptamethine dye IR-780 in the mitochondria of drug-resistant lung cancer cells. *Biomaterials* 35, 4116–4124 (2014).

70. Zhang C, Liu T, Su Y, Luo S, Zhu Y, Tan X *et al.* A near-infrared fluorescent heptamethine indocyanine dye with preferential tumor accumulation for *in vivo* imaging. *Biomaterials* 31, 6612–6617 (2010).

71. Wu C, Zhu A, Li D, Wang L, Yang H, Zeng H *et al.* Photosensitizer-assembled PEGylated graphene-copper sulfide nanohybrids as a synergistic near-infrared phototherapeutic agent. *Expert Opin. Drug Deliv.* 13, 155–165 (2016).